The index of the calculated viscous and resistive power laws is close to the 1/5 found by Poedts and Kerner (*13*) for resistive dissipation in a cylindrical loop. We found that the power law index increases when R or $S > 10^6$ (Fig. 4), in agreement with (*20*), which means that with the classical values of S and R the estimated dissipation time would be at least three orders of magnitude longer than the observed dissipation time.

The decay of the loop oscillation amplitude indicates the presence of strong dissipation of the wave energy. Dissipation leads to the heating of coronal loops. We found that as the oscillations are dissipated, the loop dims in the cooler 171 Å line (1.3×10^6 K ionization temperature), and appears to brighten in the hotter 195 Å line (1.6×10^6 K ionization temperature). This process is consistent with our understanding of the dissipation process and needs further detailed study.

If mainly the viscosity is enhanced compared with the classical value, then our results favor coronal heating by viscous dissipation of waves. Numerical simulations indicate that the classical viscosity may be enhanced by small-scale turbulence driven by fluid instabilities of the coronal plasma (*23–25*), in agreement with theoretical predictions (*9, 11*). Similarly, the enhancement of resistive dissipation requires the formation of turbulent current eddies at small spatial scales (*9*) (which in our view is less favorable for coronal loop conditions, because of the small growth rate of current instabilities compared with fluid instabilities). If the resistivity is enhanced (or the resistivity and the viscosity are enhanced), then our results support the dissipation of waves and the magnetic reconnection mechanisms for coronal heating. The difficulties that arise in these models, when the classical value of the dissipation coefficient is used, are eliminated. The fundamental plasma parameters in the solar corona are relevant to the understanding of the solar flares, to the acceleration of the solar wind and coronal mass ejection, and, ultimately, to the sun-Earth connection.

References and Notes

1. The TRACE spacecraft contains a 30-cm diameter telescope with 8.66-m Cassegrain focal length. The optics consists of superpolished mirrors individually coated in four quadrants to allow observations of the three extreme ultraviolet emission lines of 171 Å (Fe^{IX}), 195 Å (Fe^{XII}), and 284 Å (Fe^{XV}), and between 1200 and 7000 Å. Focal plane filters allow TRACE to select ultraviolet passbands around Lyman-α (1216 Å), C IV (1550 Å), the ultraviolet continuum at 1600 Å and 1700 Å, and the visible continuum up to 7000 Å wavelengths (*26*). Additional detail on the TRACE spacecraft can be found in Handy *et al.* (*27*) and at http://vestige.lmsal.com/TRACE/. First results from the TRACE mission are reported by Schrijver *et al.* (*28*) and by Golub *et al.* (*29*).
2. B. Roberts, P. M. Edwin, A. O. Benz, *Nature* **305**, 688 (1983).
3. ———, *Astrophys. J.* **279**, 857 (1984).
4. M. J. Aschwanden, L. Fletcher, C. Schrijver, D. Alexander, *ibid.*, in press.
5. J. A. Ionson, *ibid.* **226**, 650 (1978).
6. E. N. Parker, *ibid.* **264**, 642 (1983).
7. S. I. Braginskii, *Rev. Plasma Phys.* **1**, 205 (1965).
8. L. Spitzer Jr., *Physics of Fully Ionized Gases* (Interscience, New York, 1962).
9. J. Heyvaerts and E. R. Priest, *Astron. Astrophys.* **117**, 220 (1983).
10. J. M. Davila, *Astrophys. J.* **317**, 514 (1987).
11. J. V. Hollweg and G. Yang, *J. Geophys. Res.* **93**, 5423 (1988).
12. A movie made from these images is available as supplementary material at www.sciencemag.org/feature/data/1040166.shl.
13. S. Poedts and W. Kerner, *Phys Rev. Lett.* **66**, 2871 (1991).
14. R. S. Steinolfson and J. M. Davila, *Astrophys. J.* **415**, 354 (1993).
15. L. Ofman, J. M. Davila, R. S. Steinolfson, *ibid.* **444**, 471 (1995).
16. W. J. Tirry and M. Goossens, *ibid.* **471**, 501 (1996).
17. L. Ofman, J. M. Davila, R. S. Steinolfson, *ibid.* **421**, 360 (1994).
18. D. Berghmans and P. De Bruyne, *ibid.* **453**, 495 (1995).
19. P. M. Edwin and B. Roberts, *Sol. Phys.* **88**, 179 (1983).
20. L. Ofman and Z. Mouradian, *Astron. Astrophys.* **308**, 631 (1996).
21. L. Golub and J. M. Pasachoff, *The Solar Corona* (Cambridge Univ. Press, Cambridge, 1997), p. 219.
22. J. M. Kappraff and J. A. Tataronis, *J. Plasma Phys.* **18**, 209 (1977).
23. J. T. Karpen, R. B. Dahlburg, and J. M. Davila, *Astrophys. J.* **421**, 372 (1994).
24. L. Ofman, J. M. Davila, R. S. Steinolfson, *Geophys. Res. Lett.* **21**, 2259 (1994).
25. L. Ofman and J. M. Davila, *J. Geophys. Res.* **100**, 23427 (1995).
26. The optics contains an active secondary mirror with image motion compensation. Pointing is internally stabilized to 0.1 arc sec against spacecraft jitters. A 1024 by 1024 charge-coupled device (CCD) detector collects images over an 8.5 arc min by 8.5 arc min field-of-view. A powerful data handling computer enables flexible use of the CCD array including adaptive target selection, data compression, and fast operation for a limited field-of-view.
27. B. N. Handy *et al.*, *Sol. Phys.* **183**, 29 (1998).
28. C. J. Schrijver *et al.*, *ibid.*, in press.
29. L. Golub *et al.*, *Rev. Plasma Phys.*, in press.

30. We thank the TRACE team. L.O. acknowledges support by the NASA Solar Physics Supporting Research and Technology program, the NASA Space Physics Theory Program, and the NASA High-Performance Computing and Communications program. E.E.D. was supported by contract NAS5-38099 with NASA Goddard Space Flight Center. V.M.N. and B.R. acknowledge Particle Physics and Astronomy Research Council support.

18 March 1999; accepted 7 June 1999

Minimum Field Strength in Precessional Magnetization Reversal

C. H. Back,[1*] R. Allenspach,[2] W. Weber,[1] S. S. P. Parkin,[3] D. Weller,[3] E. L. Garwin,[4] H. C. Siegmann[1]

Ultrafast magnetic field pulses as short as 2 picoseconds are able to reverse the magnetization in thin, in-plane, magnetized cobalt films. The field pulses are applied in the plane of the film, and their direction encompasses all angles with the magnetization. At a right angle to the magnetization, maximum torque is exerted on the spins. In this geometry, a precessional magnetization reversal can be triggered by fields as small as 184 kiloamperes per meter. Applications in future ultrafast magnetic recording schemes can be foreseen.

Based on experimental advances, magnetization reversal has undergone considerable development in recent years. For instance, it is now possible to observe the direction of the magnetization in nanosized single-domain particles (*1–3*). In such experiments, static magnetic fields are applied. The probability that the magnetization $\vec{M}$ will reverse is determined as a function of the angle at which the external magnetic field $\vec{H}_{ex}$ is applied to the particle. The reversal mechanism is difficult to understand in detail, because $\vec{M}$ can assume complex curling and buckling modes depending on the details of the shape and magnetic properties of the particle. A conceptually simpler reversal mode is reversal by precession of the magnetization: No curling and buckling modes occur (*4, 5*). Precessional and conventional reversal differ in the angle between $\vec{M}$ and $\vec{H}_{ex}$ and in the duration of the applied field pulse. In conventional magnetic recording, for example, the reversing field is applied antiparallel to the direction of $\vec{M}$, limiting the reversal speed to the nanosecond level (*6, 7*). Much shorter reversal times can be achieved if the external magnetic field inducing the reversal is applied perpendicular to $\vec{M}$ (*4*). In this case, the magnetic field pulse induces a precessional motion of the magnetization vector that leads to magnetization reversal. Precessional reversal in the picosecond regime was demonstrated for thin films magnetized perpendicular to the film plane. However, the magnetic field had to exceed ≈2000 kA/m at a pulse length of a few pico-

[1]Laboratorium für Festkörperphysik, ETH Zürich, CH-8093 Zürich, Switzerland. [2]IBM Research Division, Zurich Research Laboratory, CH-8803 Rüschlikon, Switzerland. [3]IBM Research Division, Almaden Research Center, 650 Harry Road, San Jose, CA 95120, USA. [4]Stanford Linear Accelerator Center, Stanford University, Stanford, CA 94305, USA.

*To whom correspondence should be addressed. E-mail: back@solid.phys.ethz.ch

seconds. Here we demonstrate that considerably smaller field pulses are sufficient to reverse $\vec{M}$ in thin, uniaxial, in-plane magnetized films. In these thin magnetic sheets, the demagnetizing field $\vec{H}_D$ helps the externally applied magnetic field $\vec{H}_{ex}$ to induce magnetization reversal. When a short magnetic field pulse provokes the precession of $\vec{M}$ out of the plane of the film, a demagnetizing field $\vec{H}_D$ is induced that points normal to the surface of the film. When the external magnetic field pulse is terminated, $\vec{H}_D$ persists and the precession of $\vec{M}$ around $\vec{H}_D$ completes the magnetization reversal process. In this geometry, magnetization reversal is induced with magnetic field pulses of a few picoseconds duration, but with small field amplitudes of <200 kA/m. These amplitudes are well within reach of conventional thin-film recording heads, which are capable of producing fields on the order of 400 kA/m.

Experiments with ultrashort magnetic field pulses require thin ferromagnetic films, because the classical skin depth for the penetration of $\vec{H}_{ex}$ into a metal is $\approx$300 nm for a rise time of 1 ps. The magnetic films used in this study were made of Co with a thickness of 20 nm. Two types of Co films were used, both of which exhibited a uniaxial anisotropy in the plane of the film. One Co film (Co I) was deposited by dc magnetron sputtering on a MgO(110) substrate. Seed layers of 0.5 nm Fe/5 nm Pt were first deposited at 500°C, and subsequently the structure 10 nm Pt/20 nm Co/2 nm Pt was grown at 40°C. The other Co film (Co II) was electron beam deposited onto MgO(110) at 300°C as a 30 nm Cr/20 nm Co/2 nm Pt structure. The saturation magnetization for Co at room temperature is M_S = 1360 kA/m. The values of the uniaxial anisotropy field $\vec{H}_A$ in the plane of the films, determined using the magneto-optic Kerr effect, were 168 and 160 kA/m for Co I and Co II, respectively.

We generated the magnetic field pulses using relativistic electron bunches of the Final Focus Test Beam facility at the Stanford Linear Accelerator Center as described previously (4, 5). The finely focused electron pulse is capable of producing magnetic fields of several thousand kiloamperes per meter in strength and on a micrometer scale. The premagnetized samples were exposed to several pulses at different locations, allowing us to investigate the influence of the pulse length on identical samples. Before each run, the length of the electron pulse was selected and its spatial extent was determined at the location of the sample. The number N of electrons per pulse was recorded on a shot-by-shot basis using two toroids in the beam line. The temporal pulse lengths σ_t were 2, 3, and 4.4 ps.

The electromagnetic fields in the wake of the electron pulse generate considerable destruction in the thin film samples, but it is limited to distances $R \leq 13$ µm from the center. As shown in previous experiments (4, 5), the material remains close to ambient temperature at distances $R \geq 13$ µm. Every point in the xy plane perpendicular to the electron beam receives a magnetic field pulse of the same duration determined by σ_t. For $R \geq 13$ µm, the magnetic field $\vec{H}_{ex}$ is to a good approximation perpendicular to the radius vector $\vec{R}$ and its strength decreases as $1/R$. Before exposure, the magnetization $\vec{M}$ of the films is set along $-x$, which is the easy magnetization direction. Hence the direction of the magnetic field $\vec{H}_{ex}(x, y)$ encompasses all angles $-\pi \leq \vartheta \leq \pi$ with $\vec{M}$.

Magnetic information is then obtained in a spin-resolved scanning electron microscope (spin-SEM) (8). The magnetic pattern generated in Co I by a single field pulse of σ_t = 4.4 ps duration (Fig. 1A) shows the initial magnetization direction pointing along $-x$

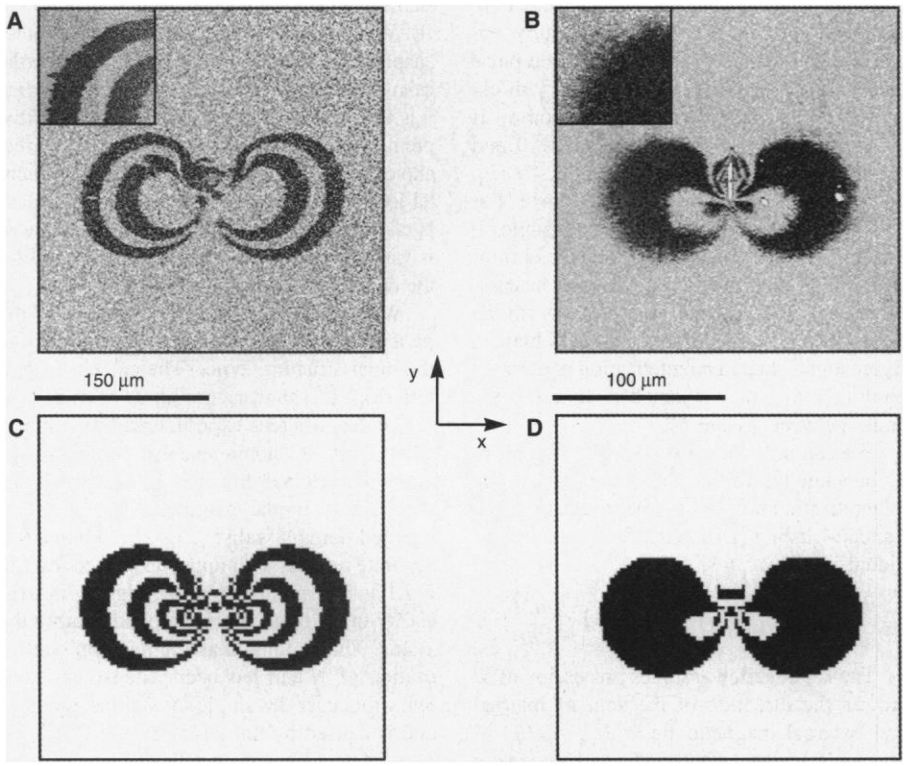

Fig. 1. (**A** and **B**) Magnetization pattern written into uniaxial cobalt films with a single electron pulse of σ_t = 4.4 ps duration. The images were measured with spin-SEM. The samples were premagnetized along the $-x$ direction. In the white areas, the magnetization points along the $-x$ direction; in the black areas it has been reversed to the $+x$ direction. (A) Image of Co I. The inset shows zig-zag domain walls separating areas of opposite $\vec{M}$. The contour lines of the pattern approximately represent lines of constant angular momentum transferred by the field pulse. (B) Image of Co II. The inset shows a gradual transition between areas of opposite $\vec{M}$. (**C** and **D**) Magnetization patterns calculated for the two different films using the LL equation with M_S = 1360 kA/m. (C) The parameters for Co I are H_A = 168 kA/m and α = 0.037, (D) whereas for Co II we use H_A = 160 kA/m and α = 0.22. The difference from (A) is caused by the increase of α.

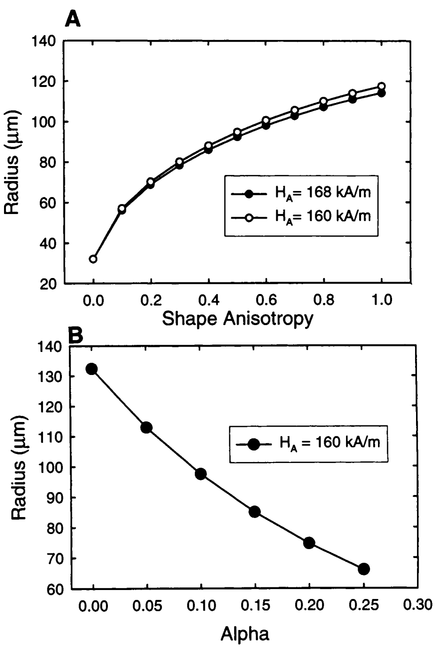

Fig. 2. (**A**) Calculated distance of the first reversal along y = 0 for σ_t = 4.4 ps and M_S = 1360 kA/m versus the difference $D_\perp - D_\parallel$ of the demagnetization factors for $\vec{M}$ perpendicular and parallel to the plane of the film for a fixed α of 0.037. (**B**) Calculated distance versus the damping constant α for $D_\perp - D_\parallel$ = 1.

(white) and the areas that have switched the magnetization direction from $-\vec{M}$ to $+\vec{M}$ (black). The location of impact is at the center of the image, which we also define as the center of the coordinate system. The induced magnetization pattern is symmetric on changing the sign of x but asymmetric on changing the sign of y.

We first concentrate on the line $y = 0$. On this line, $\vec{H}_{ex} \perp \vec{M}$ and initially the torque $\vec{H}_{ex} \times \vec{M}$ is maximum. The first reversal is $x = 110.1$ μm from the center, corresponding to a magnetic field of $H_0 = 184$ kA/m. Toward $x = 0$, which means toward larger field values, multiple reversals occur at $x = 94.2$ μm ($H_0 = 224$ kA/m), $x = 79.2$ μm ($H_0 = 264$ kA/m), and $x = 59.4$ μm ($H_0 = 352$ kA/m). On the line with zero average torque $x = 0$, no reversal is observed outside the area of beam damage. This shows the fundamental difference between conventional magnetization reversal with $\vec{H}_{ex}$ antiparallel to $\vec{M}$ and precessional reversal. For precessional reversal, the torque $\vec{H}_{ex} \times \vec{M}$ is not equal to zero and is transferred directly from the magnetic sample to the source of the magnetic field, such as the magnetic recording head. No fundamental limit seems to exist for the time interval over which the magnetic field pulse must be applied to induce magnetization reversal, given that it has the right amplitude. On the other hand, in conventional magnetization reversal, the average torque is equal to zero. In this case, the angular momentum induced by the reversal process must be absorbed by the phonon lattice, a process that is governed by the rate of energy exchange between the lattice and the magnetic system. Thus, the spin lattice relaxation time is the relevant time scale for reversal (*9*). The multiple reversals along $y = 0$ at larger field values hint at a second requirement for precessional reversal. At a given pulse length, the magnetic field strength must assume a value in a rather narrow interval, and the product $\sigma_t \times H_0$ becomes important. At this point, we also stress the size of the magnetization pattern. Its diameter amounts to 220.1 μm, about a factor of 5 larger than that observed for the perpendicularly magnetized samples in (*4*). This indicates that the field strength required for precessional reversal is considerably smaller for in-plane magnetized films, namely only 184 kA/m.

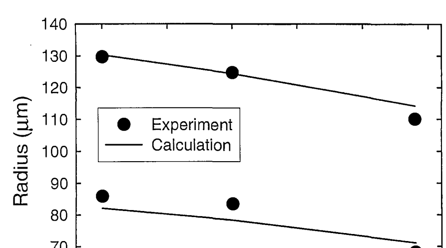

Fig. 3. Measured and calculated values of the position of the first reversal along $y = 0$ versus the length of the magnetic field pulse σ_t. The upper curve represents Co I; the lower, Co II. For the calculations, we assume $M_S = 1360$ kA/m and $D_\perp - D_\parallel = 1$. For Co I, we use $H_A = 168$ kA/m and $\alpha = 0.037$; for Co II, $H_A = 160$ kA/m, and $\alpha = 0.22$. The number of electrons per pulse was held constant in these experiments at $(9.1 \pm 0.2) \times 10^9$.

The magnetic pattern generated in Co II by an identical field pulse (Fig. 1B) shows a similar outer shape to that of Fig. 1A. However, despite having almost equal magnetic anisotropies, the pattern of Co II measures only 136.4 μm in diameter. This means that a larger field pulse amplitude is necessary to induce the first reversal, $H_0 = 312$ kA/m.

A simple model can explain why the external field needed for reversal is small. Consider a small single particle that is symmetric in the xy plane with a uniaxial anisotropy field $\vec{H}_A$ along the x direction. This particle may have any shape between a sphere and a thin disk. The corresponding demagnetizing field $\vec{H}_D$ results from the difference in the demagnetization factor $D_\parallel$ for $\vec{M}$ in the xy plane and $D_\perp$ for $\vec{M}$ along the z direction, $H_D = (D_\perp - D_\parallel)M_S/\mu_0$. Let us assume coherent rotation of $\vec{M}$ in an external field pulse of Gaussian shape applied along the y direction with an amplitude H_0 and duration σ_t. If the particle is a sphere, $D_\perp - D_\parallel = 0$ and hence $H_D = 0$. This means that for $H_0 \gg H_A$, precession of $\vec{M}$ around $\vec{H}_0$ takes place. For successful reversal, the precession angle Φ must exceed $\pi/2$, with Φ given by the Larmor frequency. This limits the radius for successful reversal to $R_0 = 32$ μm. If we now fill the plane with decoupled spheres, we obtain a figure eight–shaped magnetization pattern according to $R(x, y) = R_0 \sin(\vartheta)$, where ϑ is the angle between $\vec{M}$ and $\vec{H}_0$.

We can now increase $D_\perp - D_\parallel$ from 0 to 1, the value for a film. The calculation for the magnetization reversal is performed using the Landau-Lifshitz (LL) equation for each individual particle,

$$\frac{d\vec{M}}{dt} = -\gamma(\vec{M} \times \vec{H}_{tot}) + \frac{\alpha}{M}\left(\vec{M} \times \frac{d\vec{M}}{dt}\right)$$

The LL equation assumes precession of $\vec{M}$ around the direction of the sum of internal and external magnetic fields $\vec{H}_{tot} = \vec{H}_{ex} + \vec{H}_D + \vec{H}_A$, with γ being the gyromagnetic ratio $y = 0.2212 \times 10^6$ m/As, and relaxation of $\vec{M}$ into the field direction described by the damping constant α. We use α as the only parameter to fit the size of the pattern of Fig. 1A. The results for the two different films along $y = 0$ (Fig. 2A) show that with increasing demagnetization factor and hence increasing $H_D = M_S/\mu_0$, the size of the pattern grows rapidly. Thus, the demagnetizing field plays a crucial role in the reversal process. This leads to the following three-step model for ultrafast reversal. (i) During the field pulse, $\vec{M}$ precesses around $\vec{H}_{ex}$ out of the plane of the film. As $\vec{M}$ leaves the plane of the film, the effective demagnetizing field increases with the angle Θ between $\vec{M}$ and the film plane: $H_D = (M_S/\mu_0)\sin\Theta$. (ii) When $\vec{H}_{ex}$ ceases to exist, $\vec{M}$ continues to precess but now around $\vec{H}_D + \vec{H}_A$. The maximum angle Θ assumed by $\vec{M}$ decides whether the magnetization reverses and whether even multiple reversals can occur. (iii) Eventually $\vec{M}$ relaxes into one of the two easy magnetization directions. This final step can take up to 500 ps.

The size of the pattern for Co II is not reproduced in Fig. 2A. As both Co films have the same magnetization and demagnetization factors and similar uniaxial anisotropy, the decrease in size must be attributed to an increase in the intrinsic damping constant α (*10*). Plotting the calculated radius as a function of α for Co II with $H_A = 160$ kA/m (Fig. 2B), agreement with the experiment is reached for $\alpha = 0.22$. In the calculated magnetization patterns for Co I and Co II (Fig. 1, C and D), the difference between these two patterns is due to the different damping constants ($\alpha = 0.037$ for Co I and $\alpha = 0.22$ for Co II). We see that the size and the overall outer shape of the patterns are well reproduced by the calculation. The asymmetry of the pattern when y is inverted is caused by the direction of the premagnetization. A further test for the correct choice of α is the comparison of the experimental location of the first reversal with the calculated ones when the duration of the field pulse is varied (Fig. 3). Good agreement is found for the chosen parameters.

Whereas the size and overall shape of the pattern are well explained by the calculation, the inner structure is not. The calculated pattern (Fig. 1A) shows a multitude of rings near the center, whereas experimentally the innermost part is homogeneously magnetized along the original direction. We attribute this discrepancy to the magnetostatic energy at charged domain walls: "Zig-zag" boundaries separate regions with opposite $\vec{M}$ (see inset in Fig. 1). The amplitude of the zig-zag is largest when the boundary is perpendicular to the x axis. This is known as the head-on configuration of $\vec{M}$ and has been extensively studied. It occurs in single-crystalline samples and is caused by the large magnetostatic energy of the head-on configuration. In contrast, a regular 180° wall is formed at the boundary running parallel to the x axis. The zig-zag boundary is not reproduced by the calculation, because the long-range dipolar interaction between different cells is neglected. The calculated pattern in Fig. 1C shows that the reversed (black) part becomes increasingly thinner as the center is approached. At some point, the white areas will overlap because of the zig-zag boundaries. The overlapping leads to annihilation of the thinner black reversed areas. Such annihilation might then explain why only two black reversed areas are observed. The inset in Fig. 1B shows a gradual transition, indicating a structure dominated by grains. Owing to the reduced crystallinity of Co II, zig-zag walls are not formed. Correspondingly, a stable reversed area is seen much closer to the center of the structure.

We note that the radii of the experimentally observed inner rings are not exactly reproduced by the calculations. For example, in Co I the second reversal back to the original direction occurs at smaller field values than expected and the subsequent third and fourth reversals even more so. The same phenomenon is observed in Co II. The details of the inner structure of the patterns cannot be calculated with the simple LL approach unless one assumes that some of the material properties vary with time. Supposing that intrinsic properties such as M_S and H_A are constant, one is forced to assume that α is time dependent. Two different mechanisms might lead to a time-dependent effective damping constant α_{eff}. The first one is the excitation of magnons. The field pulses are built with frequencies close to the frequency band of magnons, hence magnon excitation might be enhanced. This can lead to an increase in energy dissipation and thus to an increase in α_{eff}. The other mechanism is electron-electron scattering (*11*). If $\vec{M}$ precesses at a different rate in each location, this scattering will be very strong, again leading to a larger effective damping constant.

Ultimately, direct observation of $\vec{M}$ during the precessional motion is desired. Freeman and co-workers (*12*) have shown that this is indeed possible with the magneto-optic Kerr effect using picosecond laser pulses. Other groups use inductive probing (*13*) or spin-polarized tunneling (*14*). Another exciting prospect comes from the development of the Next Linear Collider (*15, 16*). In this project, microstructured electron pulses will be developed that deliver a train of very strong magnetic field pulses of picosecond length, ideal for observing the dynamics of the reversal.

These results have implications for longitudinal magnetic recording and demonstrate the possibility of recording at extremely high data rates if problems arising from transitions between regions of oppositely magnetized material can be overcome. This requires a magnetic medium consisting of either identical grains or single-domain particles (*17*).

References and Notes

1. M. Ledermann, S. Schultz, M. Ozaki, *Phys. Rev. Lett.* **73**, 1986 (1994).
2. W. Wernsdorfer *et al.*, *ibid.* **78**, 1791 (1997).
3. S. Y. Chou, P. R. Krauss, L. Kong, *J. Appl. Phys.* **79**, 6101 (1996).
4. C. H. Back *et al.*, *Phys. Rev. Lett.* **81**, 3251 (1998).
5. H. C. Siegmann *et al.*, *J. Magn. Magn. Mat.* **151**, L8 (1995).
6. A. Lyberatos and R. W. Chantrell, *J. Phys. Condens. Matter* **9**, 2623 (1997).
7. W. D. Doyle, S. Stinnet, C. Dawson, L. He, *J. Magn. Soc. Jpn.* **22**, 91 (1998).
8. R. Allenspach, *J. Magn. Magn. Mat.* **129**, 160 (1994).
9. Values for the spin-lattice relaxation time are found to lie in the realm of 100 ps. A. Vaterlaus, T. Beutler, D. Guarisco, M. Lutz, F. Meier, *Phys. Rev. B* **46**, 5280 (1992); A. Scholl, L. Baumgarten, R. Jacquemin, W. Eberhard, *Phys. Rev. Lett.* **79**, 5146 (1997), and references therein.
10. α is in fact very sensitive to the quality of the sample. It is known that only high-quality samples show small damping constants. Also, the value of α might be different from values determined in ferromagnetic resonance (FMR) experiments. In FMR, a small stationary radio frequency excitation causes coherent precession around the effective field. In our experiments, in contrast, the excitation is strong and nonstationary.
11. D. Oberli, R. Burgermeister, S. Riesen, W. Weber, H. C. Siegmann, *Phys. Rev. Lett.* **81**, 4228 (1998).
12. W. K. Hiebert, A. Stankiewicz, M. R. Freeman, *ibid.* **79**, 1134 (1998).
13. T. J. Silva, T. M. Crawford, C. T. Rogers, *J. Appl. Phys.* **85**, 7849 (1999).
14. R. H. Koch *et al.*, *Phys. Rev. Lett.* **81**, 4512 (1998).
15. T. Nakanishi, in *Proceedings of LE '98*, St. Petersburg, Russia, 2 to 5 September 1998 (SPES-Lab-Publishing, St. Petersburg, Russia, 1998).
16. C. Adolphson *et al.*, "Zeroth-Order Design Report for the Next Linear Collider," Stanford Linear Accelerator Center (Stanford Univ., Stanford, CA 1996).
17. C. Stamm *et al.*, *Science* **282**, 449 (1998).

18. We gratefully acknowledge the valuable input of several people at the Final Focus Test Beam facility and Physical Electronics Laboratory, and the assistance of D. Guarisco with some of the programming. C.H.B. thanks the Swiss National Fund for financial support. This work was supported in part by the U.S. Department of Energy under contract no. DE-AC03-76SF00515.

11 January 1999; accepted 22 June 1999

Current-Induced Switching of Domains in Magnetic Multilayer Devices

E. B. Myers,[1] D. C. Ralph,[1]* J. A. Katine,[2] R. N. Louie,[2] R. A. Buhrman[2]

Current-induced switching in the orientation of magnetic moments is observed in cobalt/copper/cobalt sandwich structures, for currents flowing perpendicularly through the layers. Magnetic domains in adjacent cobalt layers can be manipulated controllably between stable parallel and antiparallel configurations by applying current pulses of the appropriate sign. The observations are in accord with predictions that a spin-polarized current exerts a torque at the interface between a magnetic and nonmagnetic metal, due to local exchange interactions between conduction electrons and the magnetic moments.

Devices containing alternating nanometer-scale-thick layers of ferromagnetic and nonmagnetic metals exhibit giant magnetoresistance (GMR), because current flow is strongly affected by the relative orientation of the magnetic moments in the layers (*1*). Specifically, antiparallel alignment of the moments gives a higher electrical resistance than parallel alignment. According to Newton's Third Law, one might also expect an inverse effect; that is, electrons scattering within the device may affect the moments in the magnets. Recent calculations indicate that spin-polarized currents flowing perpendicularly through magnetic multilayers may transfer angular momentum between layers, thereby imparting a torque on the magnetic moments (*2–5*). Experiments have found evidence of current-induced changes in the resistance of Cu/Co multilayers (*6, 7*) and granular alloys (*6*), nickel nanowires (*8*), and manganite junctions (*9*), but the nature of the excitations has not been clear. We report experimental studies using a Co/Cu/Co sandwich structure and verify the prediction of (*2*), that an applied current can be used to controllably switch magnetic domains between different orientations. As predicted by the spin-transfer theory (*2*), there is an asymmetry as a function of the direction of current bias, so that domains in the two magnetic layers can be aligned antiparallel by currents flowing in one direction, and then reoriented parallel by reversing the current flow. This effect provides a mechanism for a current-controlled magnetic memory element.

We employ a sample geometry suggested by Slonczewski (Fig. 1A) (*5*), a metal point contact adjacent to two Co layers separated by a Cu spacer. One Co layer (layer 1) is thin ($\leq$10 nm) and the other (layer 2) much thicker (100 nm), with the aim that intralayer exchange forces will make the magnetic mo-

[1]Laboratory of Atomic and Solid State Physics, Cornell University, Ithaca, NY 14853, USA. [2]School of Applied and Engineering Physics, Cornell University, Ithaca, NY 14853, USA.

*To whom correspondence should be addressed. E-mail: ralph@msc.cornell.edu